A General Filter for Stretched-Grid Models: Application in Cartesian Geometry

DORINA SURCEL AND RENÉ LAPRISE

ESCER Centre, Université du Québec à Montréal, Montréal, Québec, Canada

(Manuscript received 4 June 2010, in final form 3 November 2010)

ABSTRACT

Global climate models with variable resolution are effective means to represent regional scales over an area of interest while avoiding the nesting issues of limited-area models. The stretched-grid approach provides a dynamical downscaling approach that naturally allows two-way interactions between the regional and global scales of motion. Concentrating the resolution over a subset of the earth's surface increases computational efficiency and reduces the computational costs compared to global uniform high-resolution models; however, it does not come free of some problems related to the variation of resolution.

To address the issues associated with the stretching and anisotropy of the computational grid, a general convolution filter with a flexible response function is developed. The main feature of this filter is to locally remove scales shorter than a user-prescribed spatially varying length scale. The filtering effectiveness and computational efficiency of the filter can be custom tailored by an appropriate compromise between the filtering response and the width of the convolution stencil. This approach has been tested in one- and two-dimensional Cartesian geometry. It is shown that an effective filter can be obtained using a limited spatial stencil for the convolution to reduce computational cost, and that an adjustable spatially variable and nearly isotropic response can be obtained for application on variable grids.

1. Introduction

Regional climate modeling using a variable-resolution global approach is an alternative to the widely used nested limited-area models (LAM). A variable-resolution general circulation model (GCM) does not require lateral boundary conditions and it provides self-consistent interactions between global and regional scales of motion (Gibelin and Déqué 2003; Fox-Rabinovitz et al. 2006; Laprise 2008). Concentrating the resolution over a subset of the earth's surface increases computational efficiency, but this does not come free of some issues owing to the variation of resolution. The nonuniformity and anisotropy of the grid can result in computational artifacts and contamination of the physical solution, as does the convergence of meridians near the poles in the case of uniform latitude–longitude grids.

The technique of grid stretching is one of the most extensively used methods for implementing variable resolution in climate models. The stretched-grid (SG) approach was originally used for operational short-term numerical weather prediction (Yessad and Bénard 1996; Côté et al. 1997, 1998). The implementation of the SG approach for climate simulations was initiated in the early 1990s at Météo-France for the Action de Recherche Petite Échelle Grande Échelle (ARPEGE) spectral model (Déqué and Piedelièvre 1995) and later by other groups for gridpoint models (Fox-Rabinovitz et al. 1997; McGregor et al. 2002).

In Canada, the new generation of the Canadian Regional Climate Model (CRCM5) is being developed within the framework of the existing Global Environmental Multiscale (GEM) model presently used for global and regional numerical weather prediction at the Meteorological Service of Canada (Zadra et al. 2008). GEM supports multiple configurations, including uniform global, stretched-grid global, and nested limited area; the latter two configurations are contemplated for use in CRCM5.

Unlike the nested approach, the SG by design does not require lateral boundary conditions and it allows autonomous multiyear simulations with a single SG-GCM instead of a uniform-resolution GCM driving a nested limited-area model. The Stretched-Grid Model Intercomparison Project (SGMIP; Fox-Rabinovitz et al. 2006, 2008) in its first phase has demonstrated the ability of SG-GCM to provide good-quality regional and global climate

Corresponding author address: Dorina Surcel, Centre ESCER, Université du Québec à Montréal, Case postale 8888, Succursale Centre-ville, Montréal QC H3C 3P8, Canada.
E-mail: colan@sca.uqam.ca

DOI: 10.1175/2010MWR3531.1

simulation results. The authors mentioned the necessity of respecting some basic conditions for controlling computational problems due to grid irregularity. The following conditions must be imposed on the SG design:

- the local stretching factor, which is the ratio between adjacent grid intervals in the stretching zone, must be constant for a gradual stretching;
- the local stretching factor must not exceed 5%–10% depending on specific application;
- the maximum gridpoint distance in the low-resolution part of the domain must not exceed a few degrees in order to maintain global accuracy; and
- the grid spacing over the high-resolution area must be uniform.

Even when respecting the above constraints for the mesh design, the variation of resolution and anisotropy of the grid outside the uniform high-resolution area can result in numerical artifacts that risk contaminating the simulations. Some of these constraints, such as the local isotropy, are naturally satisfied by the conformal Schmidt transformation (Schmidt 1977) used in ARPEGE (Courtier and Geleyn 1988); other constraints, however, need to be imposed because of intrinsic limitations of resolution created by this transformation (Caian and Geleyn 1997).

Different grid structures are used in SG models based on spectral numerics (e.g., ARPEGE; Gibelin and Déqué 2003) and gridpoint discretizations [e.g., Goddard Earth Observing System (GEOS) SG-GCM; Fox-Rabinovitz et al. 1997]. In the following we will concentrate on the latter, which uses latitude–longitude stretched grids with their computational poles aligned (e.g., Fox-Rabinovitz et al. 1997) or rotated (e.g., Zadra et al. 2008) with respect to the geographical poles. Figure 1 shows a simplified sketch of a typical latitude–longitude stretched grid. The uniform high-resolution region of the domain is shown in green. The core high-resolution region is surrounded by a region where the grid is stretched in one or both directions; the stretching zones are shown in pink in Fig. 1. Beyond some distance, the grid spacing becomes constant but the mesh is then very anisotropic; these regions will be referred to as the ''arms of the cross'' and are shown in orange in Fig. 1. The domain is completed by a uniform low-resolution region shown in white in Fig. 1. (The line A–A′ will be referred to subsequently in 1D tests.)

Traditionally, two basic filtering techniques have been adapted in global variable-resolution models. A first filter is generally applied in all models formulated in longitude–latitude grids to control numerical instabilities arising from the convergence of the meridians near the poles; a polar Fourier filter (e.g., Takacs et al. 1999) is often applied in high latitudes. In stretched-grid models it is directly applied on the stretched grid, taking into account the stretching. In the GEOS SG-GCM (Fox-Rabinovitz et al. 2005) the polar filter is applied to the tendencies of the prognostic variables rather than to the prognostic variables themselves; as a result, high zonal wavenumbers are slowed down rather than being damped, which nevertheless allows the numerical stability criterion to be respected near the poles. A second filter is generally applied to remove gridpoint noise over the entire domain; this objective is reached with the application of a high-order Shapiro filter (Shapiro 1970). Takacs et al. (1999) found also that the application of a Shapiro filter with the eigenvector method produces very small differences compared to its standard application.

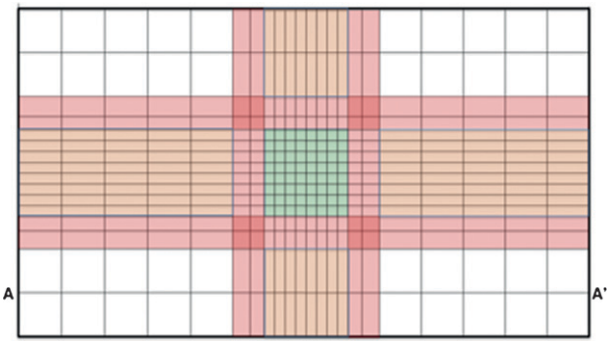

FIG. 1. Simplified sketch showing a typical latitude–longitude stretched grid. The uniform high-resolution core region of the domain is shown in green, the stretching zones are shown in pink, the anisotropic arms-of-the-cross regions are shown in orange, and the uniform low-resolution region is shown in white. The line A–A′ will be referred to subsequently in 1D variable-grid tests.

The application of a Shapiro filter on a variable-resolution grid is somewhat questionable; the filtering response being dependent on the computational grid distance, fields with a given length scale will be damped differently depending on the local mesh interval of the grid (Surcel 2005). This is what prompted us to design a method for building a general filter that can effectively remove user-defined length scales *independently of the computational mesh*. We will show that the resulting filter can be used among other applications to ensure nearly isotropic resolution even in the stretching region, and to enforce, under the control of the user, smoothly varying effective resolution over the entire domain independently of the computational mesh, including around the pole where meridians converge and the stretching zone in SG models.

This paper is organized as follows. The next section describes the formulation of the proposed general convolution filter. Section 3 presents the application of the

filter on one-dimensional uniform and stretched-grid domains, and also provides details and examples of the performance of the filter into a 2D Cartesian stretched grid. In section 4 we give some concluding remarks on the application of the filter into a Cartesian domain and general directions for the conversion of the filter to polar geometry.

2. Description of a general convolution filter

To describe the proposed convolution filter, we recall that the convolution between a signal ψ and a weighting function w can be expressed as follows, in one dimension for simplicity:

$$\overline{\psi}(x) = (\psi * w)(x) = \int_{-\infty}^{\infty} \psi(t) w(x - t)\, dt, \qquad (1)$$

where $\overline{\psi}$ represents the filtered signal and the asterisk represents convolution. The spectral response of the convolution is obtained by taking the Fourier transform of the filtered $\overline{\psi}$ and original ψ fields and evaluating the ratio of their spectral amplitudes as a function of wavenumbers. The convolution theorem (e.g., Bracewell 2000) shows that, to obtain a desired response from a convolution filter, the required weighting function is the inverse Fourier transform of that response function (e.g., Surcel 2005)

$$w(d) = \frac{1}{2\pi} \int_{-\infty}^{\infty} R(k)\, \exp(ikd)\, dk, \qquad (2)$$

where $R(k)$ is the spectral filtering response. We note that, unlike the usual gridpoint filters, the definition and properties of the convolution exist for continuous space and do not rely on the existence of a specific grid for its application; this feature will be of paramount importance for the ensuing development of the proposed general convolution filter applicable to variable-resolution grids.

The standard convolution uses a single weighting function $w(d)$ and it produces a spectral response function $R(k)$ that is constant in space. In some applications, it might be desirable to use a filter with a response function that varies with location, which we note loosely as $R(x, k)$. Modelers sometimes achieve this by using spatially varying diffusion coefficients. A simple, albeit ad hoc, modification to the standard convolution can be made to obtain a spatially varying response, consisting of using a weighting function that varies with location: $w(d, x)$. Although it is no more possible, then, to formally establish the exact response function [noted $R(x, k)$], a Wentzel–Kramers–Brillouin–Jeffreys (WKBJ) type of approximation (e.g., Bender and Orszag 1978) leads us to believe that it is reasonable to think in terms of local spectral response, as long as the weighting function varies slowly with location. Empirical evidence from the experimental results presented later will show that this approach renders sensible results even with rather rapid variations of the weighting function.

Whether on a uniform latitude–longitude grid or on a stretched grid, physical grid spacing changes with the location on the grid. On the so-called uniform latitude–longitude grid, the convergence of the meridians toward the poles induces changes in grid spacing in the zonal direction, with maximum grid spacing $\Delta x_{\max}$ near the equator. On a variable-resolution stretched grid, quasi-uniform fine mesh prevails over the area of interest, while outside this area the grid intervals increase in one or both horizontal directions. A geometric progression is often used with a constant local stretching rate defined as

$$s = \Delta x_i / \Delta x_{i-1}, \qquad (3)$$

where Δx_i and Δx_{i-1} are adjacent grid-mesh intervals. The total global stretching factor represents the ratio between the maximum and minimum grid intervals on the mesh:

$$S = \Delta x_{\max} / \Delta x_{\min}. \qquad (4)$$

A generalized convolution filter will be designed to satisfy a specific user-defined response function; this filter could be applied to control any undesirable computational noise, including that arising from the convergence of the meridians near the pole or other nonuniformity and/or anisotropy of a computational grid. Over nonuniform grids, the only waves that can be represented over the entire domain are those with length scales larger than or equal to twice the maximum grid spacing $\Delta x_{\max}$. Therefore, on a uniform latitude–longitude grid, suitable filtering could be used to remove the smaller scales in the zonal direction that are permitted by the convergence of the meridians toward the poles; this would be an effective means of ensuring computational stability as well as isotropy and homogeneity of effective resolution. Similarly, in a stretched-grid model, it would be possible to remove some anisotropic features associated with finescale structure of the mesh in only one dimension, such as in the arms-of-the-cross region surrounding the high-resolution area of interest; this may be an effective means of controlling aliasing of finescale features while they exit the high-resolution region and enter in the low-resolution part of the domain. In this case, the numerical filtering operator could suitably remove the unwanted small scales outside the uniform high-resolution area if the user so desired.

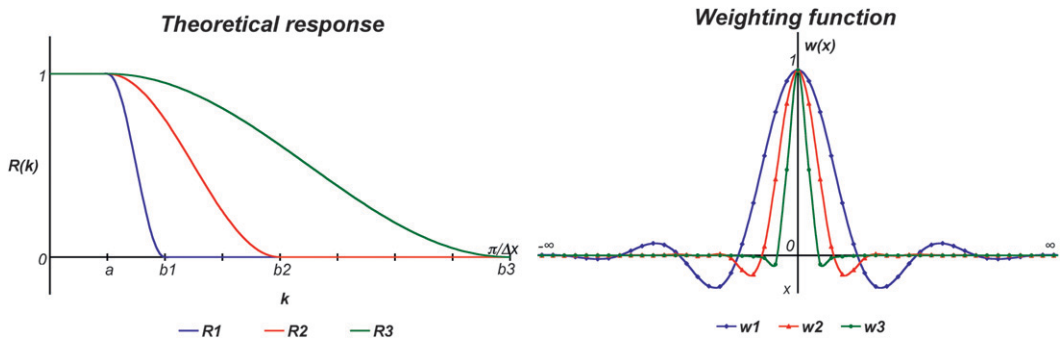

FIG. 2. (left) Examples of three different spectral responses as a function of wavenumber, and (right) corresponding weighting functions as a function of distance; the weighting functions are normalized by their maximum value.

A response function that verifies these conditions can be defined as follows:

$$R(k) = \begin{cases} 1 & 0 \le k \le a = \pi/\Delta x_{\max} \\ \cos^2 \dfrac{\pi}{2}\left(\dfrac{k-a}{b-a}\right) & a < k < b \\ 0 & b \le k \le \pi/\Delta x_{\min} \end{cases}, \quad (5)$$

which corresponds to keeping unaltered the large scales with wavenumber smaller than a (corresponding to wavelengths larger than $2\Delta x_{\max}$ that are resolved everywhere on the grid), and removing entirely small scales with wavenumber larger than a chosen value of b, with a gradual transition in between to reduce Gibbs' phenomenon. The convolution theorem then gives us the corresponding weighting function as

$$w(d) = \frac{\pi}{2}\frac{\sin ad + \sin bd}{d[\pi^2 - d^2(b-a)^2]}, \quad (6)$$

with $d = x - t$. We note in passing that a real value of response function corresponds to symmetric weighting functions.

The choice of the b parameter greatly affects the sharpness of the spectral response and the width of the weighting function, as illustrated in Fig. 2 for three values of b. A relatively small value of $b - a$, corresponding to a narrow response transition such as R1, gives rise to a broad weighting function (w_1) with oscillating values over a large segment of the domain. On the other hand, a more localized weighting function such as w_3 corresponds to very gradual response function R3.

Although the formal definition of the convolution (1) exists for continuous space, its practical application requires a version to be defined using a discrete set of points $(x_i)_{i=1,n}$ on a grid. The following general trapezoidal quadrature can be used as follows:

$$\overline{\psi}(x_i) = \frac{\sum_{j=-\infty}^{\infty} \psi(x_j) w(d_{i,j}) \sigma(x_j)}{\sum_{j=-\infty}^{\infty} w(d_{i,j}) \sigma(x_j)}, \quad (7)$$

where $\sigma(x_j)$ is a variable weight assigned to the contribution of each computational point $\sigma(x_j) = (x_{j+1} - x_{j-1})/2$ to account for the stretching. We want to stress that the convolution weights are a function of the *physical* distance $d_{i,j} = |x_i - x_j|$ between the application point x_i and all other contributing points x_j. The use of physical distance is the distinguishing feature of the proposed approach. In conventional gridpoint filtering such as the Shapiro filter, the weights are function of the indices ($|i - j|$) rather than physical distance. While both approaches render the same results on uniform grid, the use of physical distance in the convolution offers definite advantages over variable grids, as we shall demonstrate.

Returning to the weighting function $w(d)$ (e.g., Fig. 2), clearly the presence of nonvanishing values over the entire domain is problematic in practice because of the excessive computational cost. By inspection of the weighting function curve, however, one notices that values become rather small and alternate in sign after some distance from the origin. Hence in the following, we will test various pragmatic approximations to R consisting of truncating w to zero after some distance $d_{\max}$ from the origin, aiming at important reduction in computational cost. Therefore, the filtering formula will be approximated as

$$\overline{\psi}(x_i) = \frac{\sum_{d_{i,j} \le d_{\max}} \psi(x_j) w(d_{i,j}) \sigma(x_j)}{\sum_{d_{i,j} \le d_{\max}} w(d_{i,j}) \sigma(x_j)}. \quad (8)$$

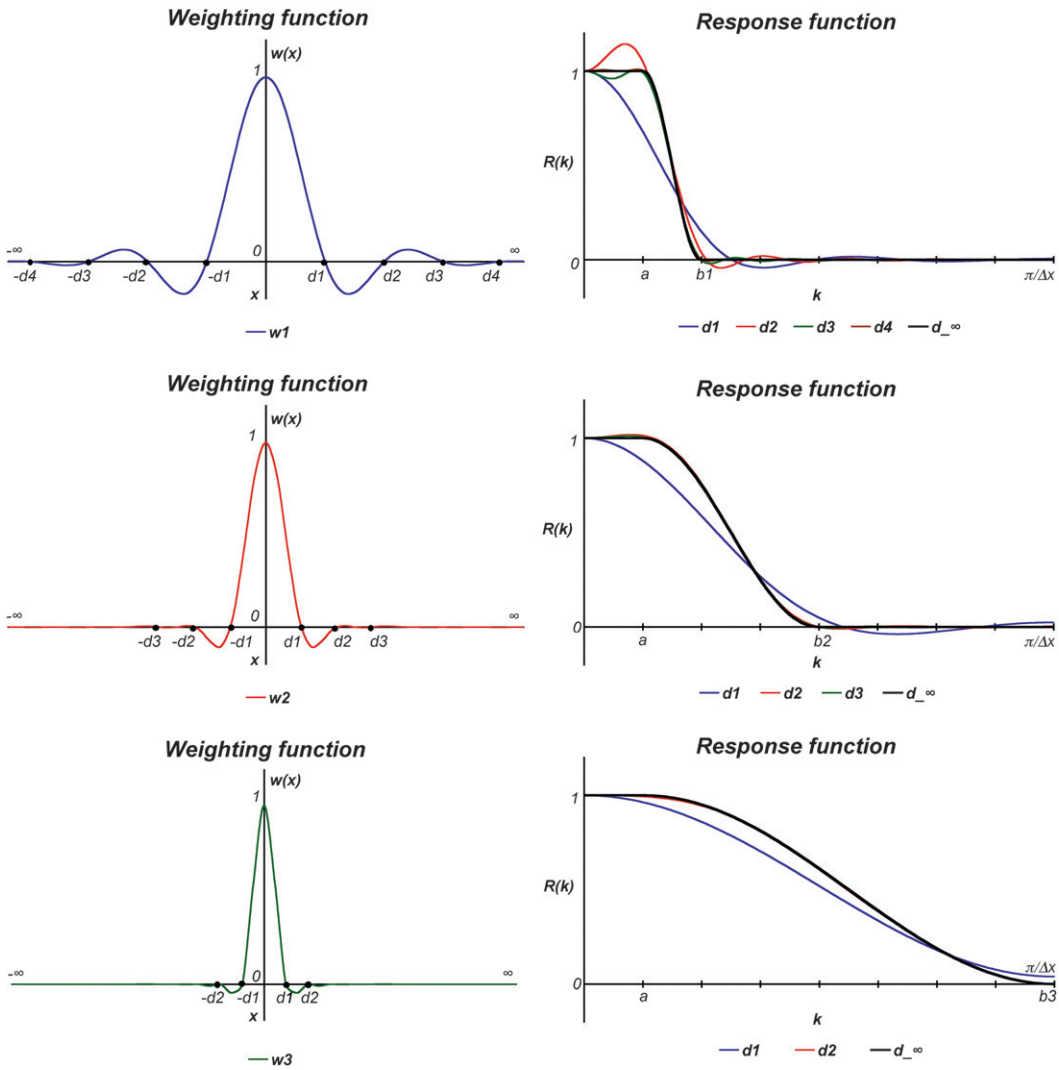

FIG. 3. (left) The three weighting functions represented in Fig. 2 with the location of various arbitrary truncation distances noted d_1 to d_4. (right) The corresponding spectral responses obtained after the application of the convolution filter with the truncated weighting functions; the exact responses are the curves in black labeled d_∞.

The three weighting functions represented in Fig. 2 will successively be tested considering different values of the cutoff distance $d_{\max}$. We will study the impact on the corresponding response function of using four cutoff distances (d_1, d_2, d_3, and d_4) as indicated in Fig. 3. The first case corresponds to a wide-footprint weighting function w_1 (Fig. 3, upper panels). We note that the theoretical response (represented by the curve d_∞) is adequately approximated only with large cutoff distances; otherwise, the response of the filter shows large oscillations corresponding to false amplification or attenuation of the field.

Narrower weighting functions such as w_2 (Fig. 3, middle panels) are much less demanding; a relatively adequate response function is obtained with much smaller cutoff distance, and there is little difference in the response for cutoff distance $d_{\max} > d_2$. An even better approximation is obtained for w_3 with a much smaller cutoff distance (Fig. 3, bottom panels). This weighting function corresponds to the most gradual variation of the spectral response in our test case.

In summary, the choice of the weighting function is very important for two main reasons. First, a weighting function corresponding to an abrupt change in the spectral response contains large oscillations and needs a large cutoff distance, which would translate to increased computational costs. Second, a gradually varying response function gives rise to a narrow weighting function and thus to a much smaller acceptable cutoff distance in order to approximate adequately the theoretical response.

In this case, we must be aware that only a small part of the spectrum is completely removed—the rest being only attenuated. This is not necessarily a problem, as we will see later, because repeated applications of such a filter (as it would be the case if the filter is applied at every time step during the integration of the model) would be as effective at removing undesired scales as a wider weighting function but at a lesser computational cost.

In the next section we will test different weighting functions and will discuss the advantages and disadvantages for the use of different filter configurations.

3. Applications

This section presents some examples of applications of the proposed convolution filter into 1D and 2D Cartesian domains, initially with uniform resolution and later with a stretched grid. We express the 1D test function as $\psi(x) = \psi_l(x) + \psi_n(x)$, where ψ_l is a large-scale wave representing the physical signal that is properly represented on the entire domain, and ψ_n is a small-scale wave representing noise. The filter will be aimed at maintaining the large-scale signal but at attenuating or removing the small-scale noise.

The skill of the filter will be quantitatively evaluated by comparing the filtered solution $\overline{\psi}$ with the expected analytical solution ψ_l using two scores: the normalized root-mean-square (NRMS) error and the normalized conservation ratio (NCR). The root-mean-square error will be computed between the filtered solution and the expected analytical solution (after subtracting the mean error) and normalized by the variance of the analytical solution

$$\mathrm{NRMS} = \frac{\sqrt{\sum_k [\overline{\psi}(x_k) - \psi_l(x_k) - \overline{\Psi}]^2 \sigma(x_k)}}{\sqrt{\sum_k [\psi_l(x_k)]^2 \sigma(x_k)}}, \quad (9)$$

where $\overline{\Psi} = \sum_k [\overline{\psi}(x_k) - \psi_l(x_k)]\sigma(x_k)/\sum_k \sigma(x_k)$ is the domain-averaged error between the filtered solution and the analytical solution. The NCR checks mass conservation as the mean error between the filtered and unfiltered solution and is normalized by the variance of the analytical solution

$$\mathrm{NCR} = \frac{\sum_k [\overline{\psi}(x_k) - \psi(x_k)]\sigma(x_k) \Big/ \sum_k \sigma(x_k)}{\sqrt{\sum_k [\psi_l^2(x_k)\sigma(x_k)] \Big/ \sum_k \sigma(x_k)}}. \quad (10)$$

For all the tests, we used a function in the form of a sum of single harmonics for both the large-scale signal and small-scale noise

$$\psi(x_i) = A_l \cos(k_l x_i) + A_n \cos(k_n x_i), \quad (11)$$

where A_l and A_n are arbitrarily constants, and k_l and k_n are wavenumbers of the signal to be retained and the noise to be removed, respectively. In the following, we will use the convention that x covers the interval from 0 to 2π.

a. Application of the convolution filter in a 1D uniform domain

A necessary condition for any filtering method proposed for a variable mesh is to perform adequately for a uniform grid. In this section, we test the performance of various configurations of the convolution filter in idealized conditions on a uniform-resolution 1D domain.

Three test functions will be used, noted ψ_1, ψ_2, and ψ_3, defined on 256 grid points so that $256\Delta x = 2\pi$. All test functions will use the same signal with wavenumber $k_l = 2(2\pi/256\Delta x) = 2\pi/128\Delta x$ corresponding to two oscillations around the periodic domain and a wavelength of $\lambda_l = 128\Delta x$. Three test functions will be used with different noise scales characterized by the following wavenumbers and wavelengths: $k_{n_1} = 32(2\pi/256\Delta x) = 2\pi/8\Delta x$ and $\lambda_{n_1} = 8\Delta x$ for the first, $k_{n_2} = 64(2\pi/256\Delta x) = 2\pi/4\Delta x$ and $\lambda_{n_2} = 4\Delta x$ for the second, and $k_{n_3} = 128(2\pi/256\Delta x) = 2\pi/2\Delta x$ and $\lambda_{n_3} = 2\Delta x$ for the third test function.

There are three main parameters that control the response of the filter as defined: a and b characterize the formal filtering response (large scales with wavenumbers smaller than a are kept intact while small scales with wavenumbers larger than b are removed entirely, with a gradual transition in between), and the finite width of the stencil $d_{\max}$ affects the accuracy of the actual filter. We will use a single value for the parameter $a = 2\pi/16\Delta x = 16(2\pi/256\Delta x)$, corresponding to an ideal response in which all length scales larger than or equal to $16\Delta x$ are kept. We will vary the b parameter as $b_1 = 2a = 2\pi/8\Delta x = 32(2\pi/256\Delta x)$, $b_2 = 4a = 2\pi/4\Delta x = 64(2\pi/256\Delta x)$, and $b_3 = 8a = 2\pi/2\Delta x = 128(2\pi/256\Delta x)$, which corresponds to removing all length scales shorter than or equal to $8\Delta x$, $4\Delta x$, and $2\Delta x$, respectively. These choices parameters correspond to three weighting functions in the convolution formulation w_1, w_2, and w_3, as shown in the left panels of Fig. 3. We will assess the performance of the filters on the test functions using various stencil widths.

Figure 4 shows visually the results of the three filters applied on ψ_1 (Figs. 4a,c,e) and ψ_2 (Figs. 4b,d,f) using a stencil that is wide enough to approximate well the theoretical response as seen in Fig. 3. The first filter (using b_1) was designed in such a way that it should remove entirely the noise for both ψ_1 and ψ_2 test functions because $b_1 \leq (k_{n_1}, k_{n_2})$; Figs. 4a,b confirm the expectation. In this case the truncation distance $d_{\max} = d_4 = 21\Delta x$ was

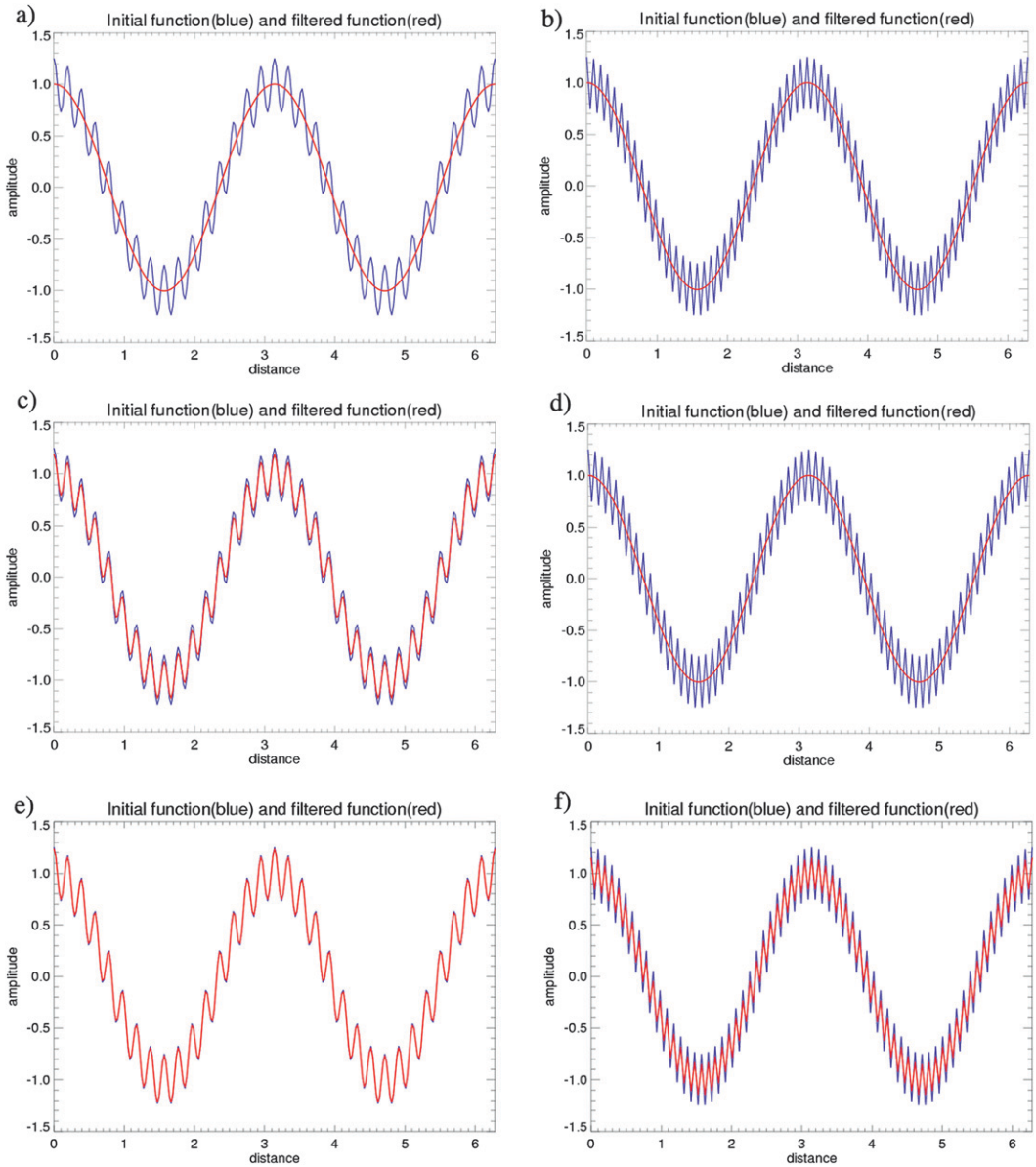

FIG. 4. Test functions (left) ψ_1 and (right) ψ_2 in blue and the filtered fields in red. (a),(b) The filter used the weighting function w_1 and a truncation distance of $21\Delta x$; (c),(d) the filter used the weighting function w_2 and a truncation distance of $10\Delta x$; and (e),(f) the filter used the weighting function w_3 and a truncation distance of $4\Delta x$.

used in w_1 (see the upper-left panel in Fig. 3). The second filter (using b_2) was designed such as to remove entirely the noise of ψ_2 because $k_{n_2} \geq b_2$, but only attenuate weakly the noise of ψ_1 because $k_{n_1} < b_2$; Figs. 4c,d again confirm the expectation. Because this second filter has a broader spectral response, a shorter truncation distance $d_{\max} = d_3 = 10\Delta x$ was sufficient to approximate w_2, as seen in the middle-left panel of Fig. 3. The third filter (using b_3) was designed to only attenuate the noise of ψ_1 and ψ_2 because $(k_{n_1}, k_{n_2}) < b_3$; Figs. 4e,f confirm the expectation, and in fact this filter has very little effect on ψ_1. Because this third filter has an even broader spectral response, a very short truncation distance $d_{\max} = d_2 = 4\Delta x$ was sufficient to approximate w_3, as seen in the lower-left panel of Fig. 3. We note that all three filters were very effective in removing entirely the noise in the third test function ψ_3 characterized by $2\Delta x$ short-scale noise, and for this reason the figures are not shown.

We now proceed to the quantitative evaluation of the filtering response for the three test functions ψ_1, ψ_2, and ψ_3. In Fig. 5, the NRMS is shown as a function of the truncation distance used for the stencil in the

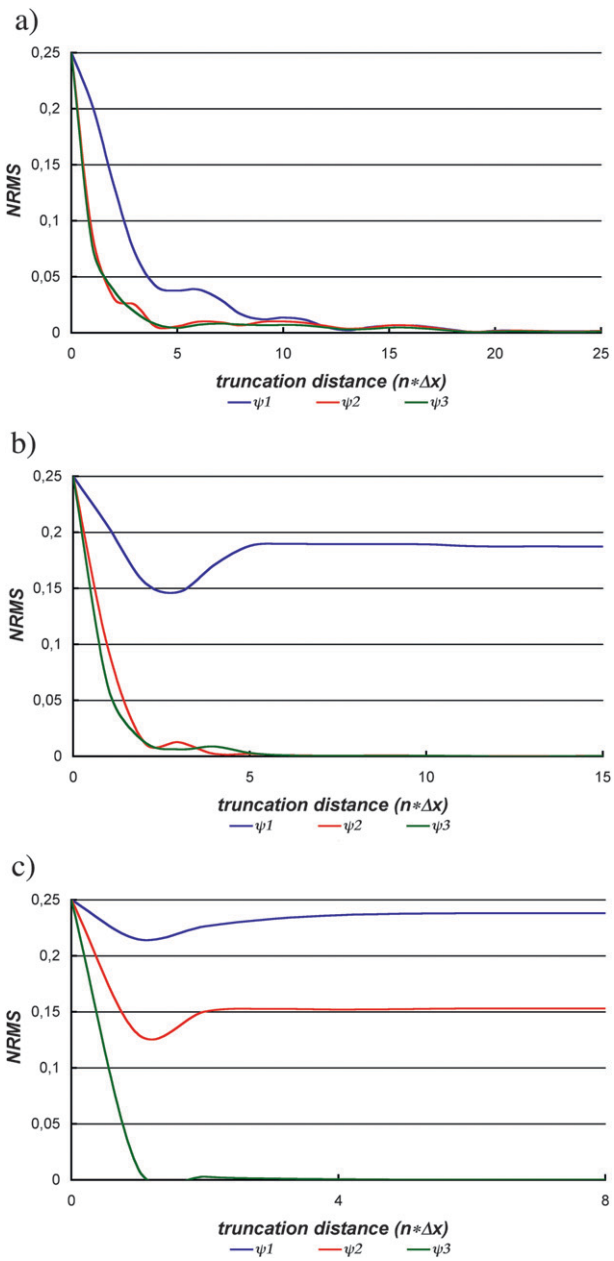

FIG. 5. Variation of the NRMS scores as a function of the truncation distance for the test functions ψ_1, ψ_2, and ψ_3, using the weighting functions (a) w_1, (b) w_2, and (c) w_3.

convolution. In the case of the first filter with a sharp spectral response function and, therefore, a broad weighting function w_1, the noise is completely removed only if the truncation distance is large enough to approximate the theoretical response (Fig. 5a). The other two filters have more gradual response functions and thus narrower weighting functions w_2 and w_3; in this case, the NRMS converges more rapidly to the value that represents the amplitude of the noise remaining after filtering according to the theoretical response in the definition of the weighting function (Figs. 5b,c).

In all cases, the conservation ratio was verified and the NCR scores were within the round-off error of the computer used for these tests.

We note that a sharp spectral response to the filter implies a broad-structure weighting function in the convolution, and that the increase of the stencil width improves the accuracy of the filter, which is then able to produce the theoretical response. But this increase of stencil width has drawbacks: first, it is computationally expensive (especially in many dimensions); and second, it involves large volumes of data motion for implementation on distributed-memory parallel computers. Narrower stencils are computationally more efficient in the convolution, but with very narrow stencils, the filter only approximates the theoretical response, which may result in reducing the amplitude of the noise one wishes to eliminate—but without removing it entirely as in the theoretical response. In practice, however, filters can be applied at time intervals—possibly at every time step—in atmospheric models. The repeated application of a less-expensive filter using a narrow stencil, which only damps without suppressing entirely undesired noise, can be as efficient and effective as a more accurate but expensive filter using a wide stencil.

We proceed to illustrate the effect of repeated application of a filter. We recall that the third filter (using b_3) was designed such as to remove entirely the noise in the third test function ψ_3 characterized by very short-scale noise with wavenumber k_{n_3}, but to only attenuate the larger-scale noise of ψ_1 and ψ_2; in fact, this filter had a very weak damping effect on the noise of ψ_1. Figure 6a shows the response of the repeated application of the filter. The small-scale noise of the test function ψ_2 with wavenumber k_{n_2} is essentially eliminated after 10 applications. For the test function ψ_1, the noise with wavenumber k_{n_1} still remains even after 40 applications, and we also note a small attenuation of the large-scale signal (at wavenumber a) caused by the repeated applications of the filter. The variation of the NRMS for the noise component as a function of the number of applications of the filter to ψ_1 and ψ_2 is shown in Fig. 6b. Figure 7 shows the results on test function ψ_2 after 4 and 10 applications (Figs. 7a,b), and on test function ψ_1 after 4 and 40 applications. As expected, this particular choice of compact filter is more effective at damping short-scale noise than larger-scale one, but repeated application of the filter succeeds at reducing substantially even larger-scale noise.

b. *Application of the convolution filter into a 1D stretched grid*

The application of the convolution filter for a variable-resolution domain is tested considering a periodic 1D

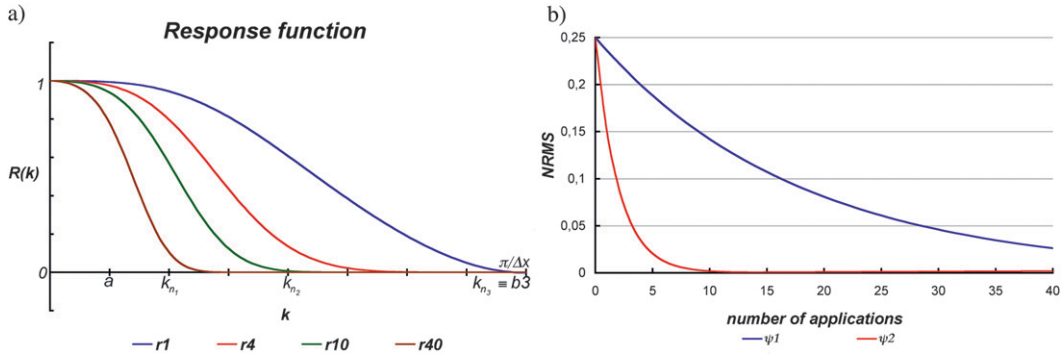

FIG. 6. (a) Spectral response after 1, 4, 10, or 40 applications of the convolution filter using weighting function w_3. The wavenumbers corresponding to the test functions ψ_1, ψ_2, and ψ_3 are indicated on the horizontal axis. (b) The NRMS score as a function of the number of applications of the convolution filter using weighting function w_3 on the test functions ψ_1 and ψ_2.

stretched grid. The domain $[0, 2\pi]$ is divided into four main zones: a uniform fine-resolution zone with grid mesh $\Delta x_{\min}$ located in the center of the domain, bordered by two stretching zones where the resolution is gradually degraded, and completed by a uniform low-resolution zone with grid mesh $\Delta x_{\max}$, as represented in Fig. 8. Such a configuration is typical of the varying resolution around a latitude circle in the region outside the uniform high-resolution area of the domain, as indicated for example by the line segment A–A′ in Fig. 1, which slices through the arms-of-the-cross region in the latitude–longitude grid.

One purpose of the 1D stretched-grid tests will be to verify the ability of the general convolution filter to

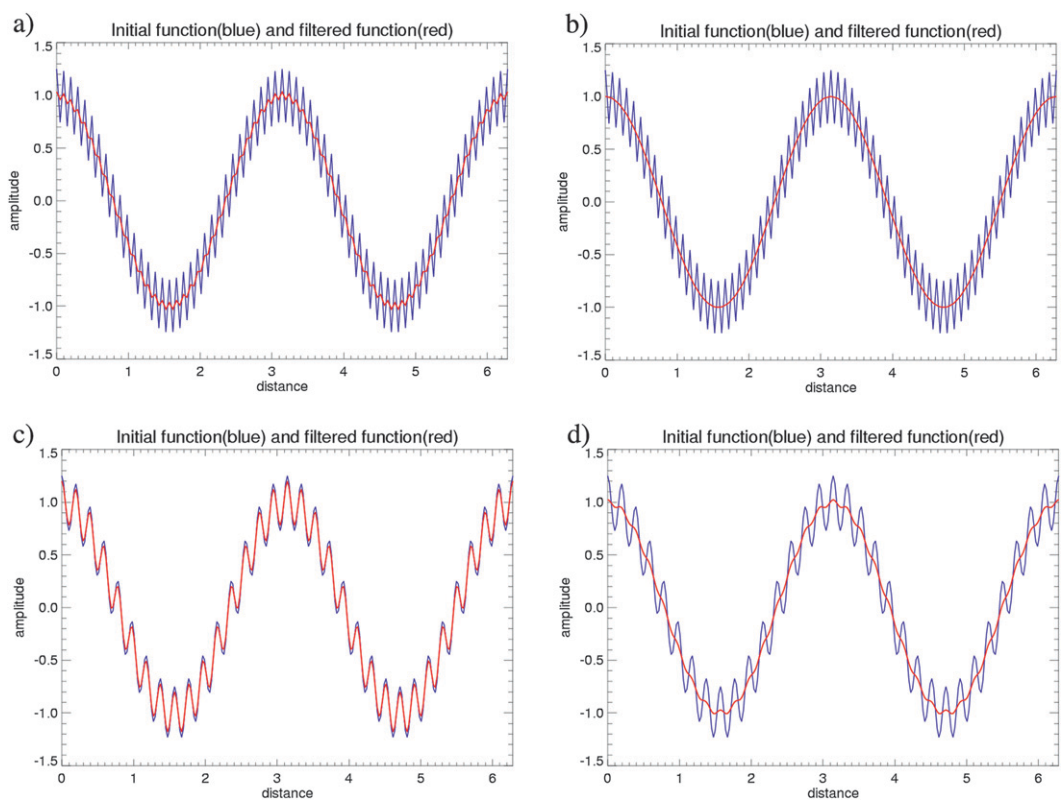

FIG. 7. (top) The initial test function ψ_2 (blue) and the filtered field (red) after (a) 4 and (b) 10 applications of the convolution filter with weighting function w_3 and truncation distance $d_{\max} = 4\Delta x_{\min}$. (bottom) The corresponding results for test function ψ_1 after (c) 4 and (d) 10 applications of the same convolution filter.

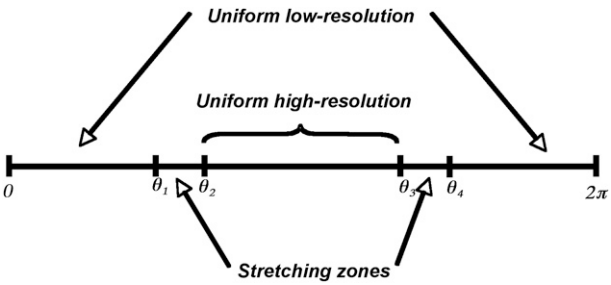

FIG. 8. General configuration of the 1D stretched grid.

TABLE 1. Parameters of 1D stretched grids used to verify the performance of the convolution filter.

	High-resolution zone	Stretched-grid zones	Local stretching factor «s»	Total stretching factor «S»
SG1	$\left[\frac{2\pi}{3}, \frac{4\pi}{3}\right]$	$\left[\frac{7\pi}{12}, \frac{2\pi}{3}\right] \cup \left[\frac{4\pi}{3}, \frac{17\pi}{12}\right]$	7.2%	4
SG2	$\left[\frac{2\pi}{3}, \frac{4\pi}{3}\right]$	$\left[\frac{5\pi}{12}, \frac{2\pi}{3}\right] \cup \left[\frac{4\pi}{3}, \frac{19\pi}{12}\right]$	2.4%	4

actually render uniform-resolution fields despite the varying grid mesh. If effective, such a filter could be used in 2D to remove the anisotropy of the grid in the arms-of-the-cross region of the grid. The test functions used for the following 1D stretched-grid tests are in the form analogous to (11) that was used for the uniform resolution, but here the noise amplitude is chosen to be zero in the low-resolution part of the domain, gradually increased in the stretching areas, and is maximum in the high-resolution area that is here taken to represent the anisotropic-grid arms-of-the-cross region of a 2D domain. Two grid designs will be used in the following experiments (see Table 1). We mention in passing that for both grids, the number of grid points located in the uniform high-resolution area represents 60%–64% from the total number of grid points, even if the area represents only 1/3 from the entire domain.

In the following tests, we will interpret the high-resolution part of the 1D grid as corresponding to the anisotropic arms-of-the-cross region of a 2D grid; the convolution will be applied with the aim of filtering some small-scale noise that a user may want to remove outside the uniform high-resolution zone. Therefore, in our 1D variable domain, the filter will be designed to render quasi-uniform-resolution fields by removing scales with wavelengths shorter than twice the maximum grid mesh in the domain; consequently, the parameter a in the weighting function, which controls the largest wavenumber retained on the entire grid, is chosen as $a = 2\pi/2\Delta x_{\max}$. Various values of the parameters b and $d_{\max}$ will be tested and results will be presented through examples of filtered functions and NRMS and NCR statistics for the two stretched grids mentioned above.

A first example is shown for grid SG2 in Fig. 9. In this case, the test function contained a noise with wavenumber $k_n = 2\pi/4\Delta x_{\min}$. A convolution filter w_1 was chosen to completely remove the smallest resolved scale in the high-resolution region using parameter $b = 1.5a$; therefore, $k_n < b$. Figure 9 shows the result obtained with a truncation distance $d_{\max} = 5\Delta x_{\max}$ for the weighting function. We see that the goal is reached: the short-scale noise is completely removed and the large-scale signal perfectly maintained.

We study the effects of different stretching rates by running tests on two variable-resolution grids—SG1 and SG2—that have the same total stretching factor ($S \cong 4$), but the stretching rate of SG1 is 3 times larger than that of SG2. We will use the same test function as in the previous case, and use two convolution filters aiming at removing entirely small-scale noise, with weighting functions w_1 ($a = 2\pi/2\Delta x_{\max}$; $b = 1.5a$) and w_2 ($a = 2\pi/2\Delta x_{\max}$; $b = 2a$). The NRMS scores are shown in Fig. 10a. It is seen that the noise is completely removed if an adequate truncation distance is used; this distance is shorter for the filter with the more gradual response (w_2). There appears to be little impact of the stretching rate on the NRMS score. For the NCR score (Fig. 10b), we note that better conservation is obtained with the filter with the more gradual response (w_2) and on the grid with smaller stretching rate (SG2).

As mentioned before, a large truncation distance permits one to completely remove scales smaller than b and

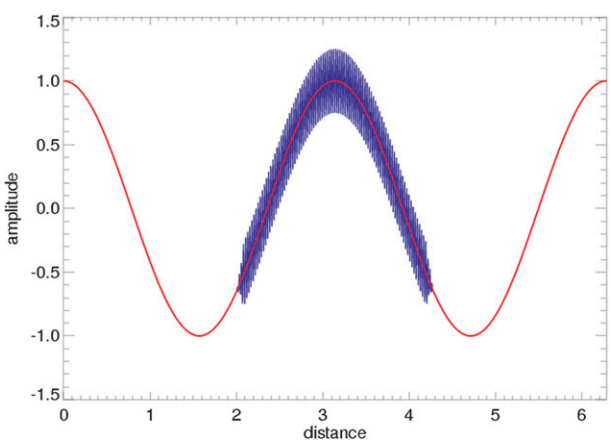

FIG. 9. The initial test function (blue) and the filtered field (red) on the SG2 grid with $S \cong 4$. For the convolution, the weighting function used parameters $a = 2\pi/2\Delta x_{\max}$ and $b = 1.5a$, and a truncation distance $d_{\max} = 5\Delta x_{\max}$; the noise in the test function had a wavenumber of $k_n = 2\pi/4\Delta x_{\min}$.

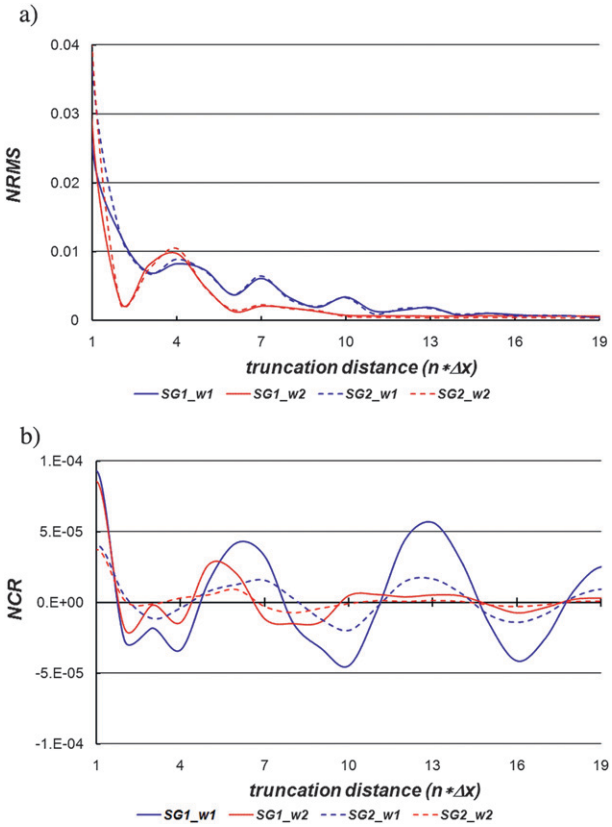

FIG. 10. The (a) NRMS and (b) NCR scores as a function of the truncation distance for two convolution filters with weighting functions w_1 ($a = 2\pi/2\Delta x_{\max}$; $b = 1.5a$) and w_2 ($a = 2\pi/2\Delta x_{\max}$; $b = 2a$), applied on SG1 and SG2 stretched grids.

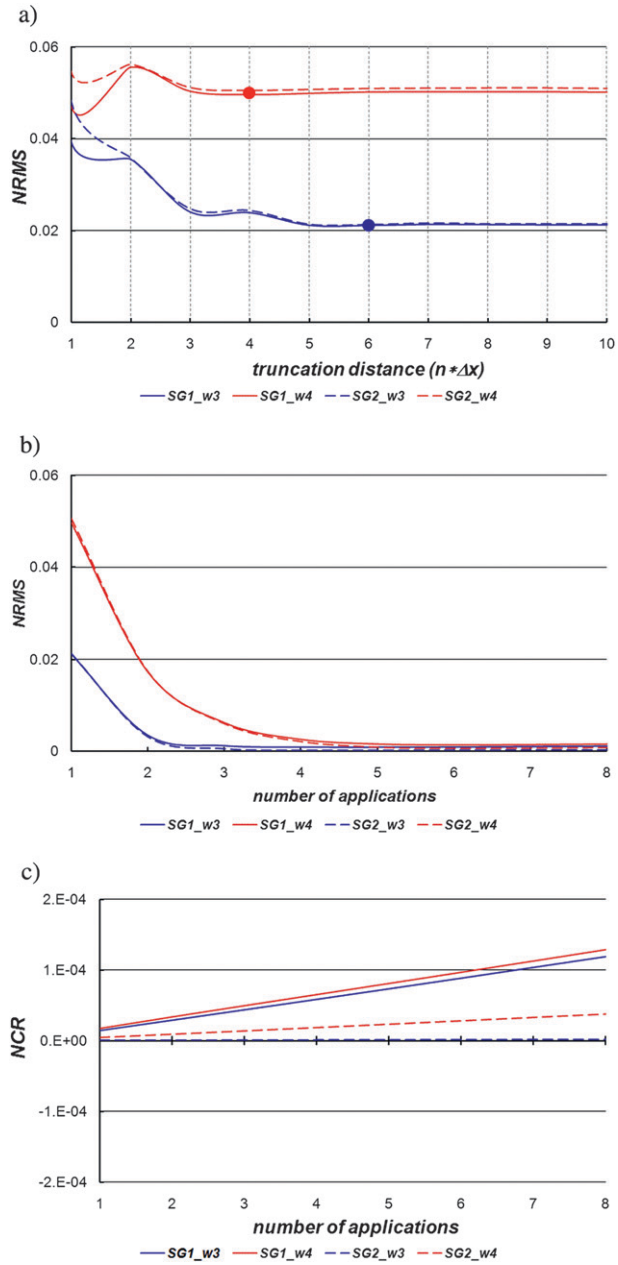

FIG. 11. (a) The NRMS score as a function of the truncation distance for two convolution filters with weighting functions w_3 ($a = 2\pi/2\Delta x_{\max}$; $b = 3a$) and w_4 ($a = 2\pi/2\Delta x_{\max}$; $b = 3.5a$), applied on SG1 and SG2 stretched grids. (b) The NRMS score as a function of the number of application of convolution filters with weighting functions w_3 with a truncation distance of $6\Delta x_{\min}$, and w_4 with a truncation distance of $4\Delta x_{\min}$. (c) As in (b), for the NCR score.

maintain conservation, but wide stencils come with increased computational costs. For this reason, it may be preferable to use convolution filters using weighting function with a narrow stencils, even if such filters remove only a fraction of the noise at every application.

For the next experiment, we use the same test function and stretched grids, and apply two convolution filters with theoretical response corresponding to removing only a fraction of the noise at every application, with weighting functions w_3 ($a = 2\pi/2\Delta x_{\max}$; $b = 3a$) and w_4 ($a = 2\pi/2\Delta x_{\max}$; $b = 3.5a$) corresponding to stronger and weaker filtering of the shorter scales, respectively. The truncation distance used for these applications was $6\Delta x_{\min}$ for w_3 and $4\Delta x_{\min}$ for w_4. Figure 11a shows that the NRMS score initially decreases as a function of the truncation distance, but—after a certain truncation distance—it becomes constant but not zero, meaning that a part of the noise is still present; increasing the truncation distance will not improve the score because the response of the filter then reproduces exactly the theoretical response corresponding to removing only a fraction of the noise. To remove completely the noise using such weighting functions, the filter must be repeatedly applied. Figure 11b shows the NRMS score with repeating the application of the filter; for these tests, we chose the truncation distance for which the NRMS was nearly constant, indicated by the dot in Fig. 11a. We can see that just after few applications the NRMS

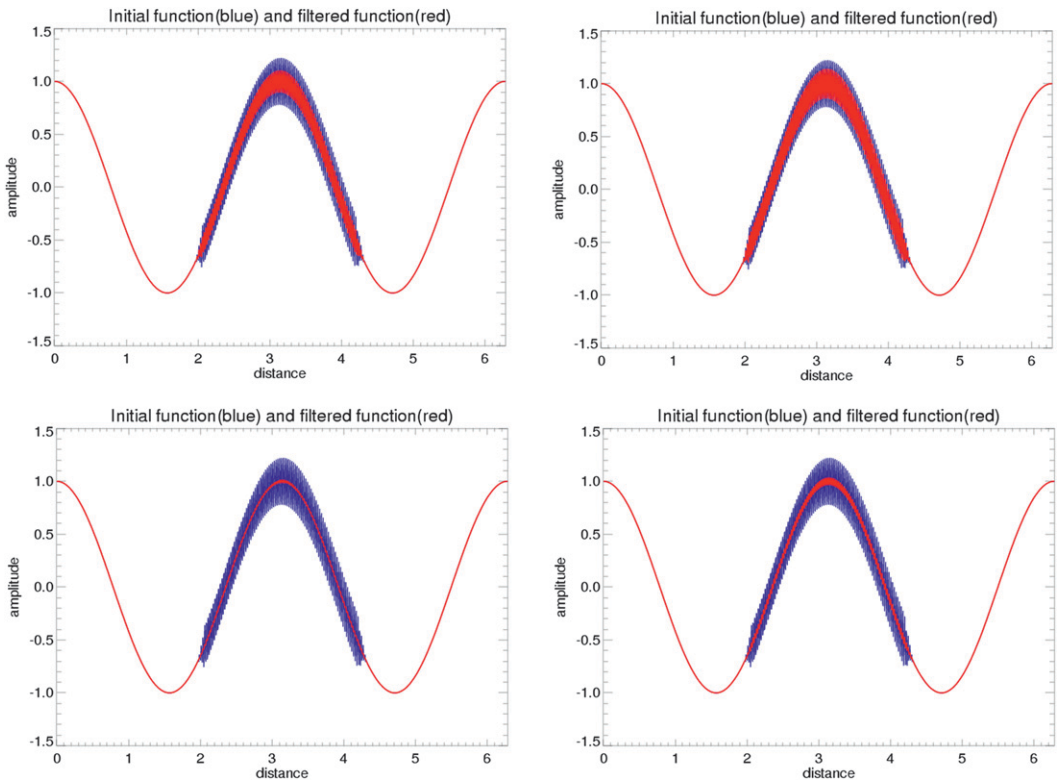

FIG. 12. The initial test function (blue) with noise of wavenumber $k_n = 2\pi/4\Delta x_{\min}$ on the SG2 grid, and the filtered field (red) after 1 (first row) and 4 applications (second row) of the convolution filter. (left) Results obtained using a weighting function w_3 with parameters ($a = 2\pi/2\Delta x_{\max}$; $b = 3a$) and a truncation distance of $8\Delta x_{\min}$, and (right) a weighting function w_4 ($a = 2\pi/2\Delta x_{\max}$; $b = 3.5a$) with a truncation distance $d_{\max} = 6\Delta x_{\min}$.

is almost zero. We note, however, a slight but systematic attenuation of the largest scales with several applications of the filter; this shows in Fig. 11b as a nonzero value of NRMS and in Fig. 11c as a linear increase of NCR for repeated applications. The mass nonconservation is particularly pronounced for the grid with the larger stretching rate (SG1) and for the less scale-selective filter (w_4).

We next illustrate the results of the convolution filter on SG2 using the same test function that was used in Fig. 9, with a noise characterized by wavenumber $k_n = 2\pi/2\Delta x_{\min}$. In Fig. 12, the blue and red lines represent the initial and the filtered functions, respectively. The left column shows results for the weighting function w_3 ($a = 2\pi/2\Delta x_{\max}$; $b = 3a$) with a truncation distance $d_{\max} = 8\Delta x_{\min}$, and the right column for w_4 ($a = 2\pi/2\Delta x_{\max}$; $b = 3.5a$) with a truncation distance $d_{\max} = 6\Delta x_{\min}$; the first row shows results after one application of the filter, and the second row after four applications. After one application of the w_3 filter, the amplitude of the noise is reduced by 52%, and after four applications only 5% of the noise remains. For comparison, after one application of the w_4 filter, 36% of the noise is removed, and after four applications 17% of the noise is still present.

A general filtering technique applied on a variable-resolution domain must be able to remove at the same time any noise that may result from the anisotropy in the stretching zones, but also the computational noise characteristic of any numerical model. We next consider a test function composed from three harmonics. The first one represents a large-scale signal to be preserved under filtering. The second harmonic represents a computational noise present anywhere on the grid. The third one represents another noise that may be resulting from the stretching of the grid; we will introduce it only in the stretching region and the high-resolution area that we will interpret here as corresponding to the anisotropic arms-of-the-cross region of a 2D grid. We used the following test function:

$$\psi(x_i) = A_l \cos(k_l x_i) + A_{n_l} \cos(k_{n_l} x_i) + A_{n_h} \cos(k_{n_h} x_i),$$

where A_l, A_{n_l}, and A_{n_h} are arbitrary amplitudes, and k_l, k_{n_l}, and k_{n_h} are the wavenumbers of the large-scale signal and of the two types of noises.

For the test shown in Fig. 13, we used the values $k_l = 2(2\pi/256\Delta x_{\max}) = 2\pi/128\Delta x_{\max}$, $k_{n_1} = 2\pi/4\Delta x_{\max}$, and $k_{n_2} = 2\pi/4\Delta x_{\min}$, and a convolution filter with a weighting

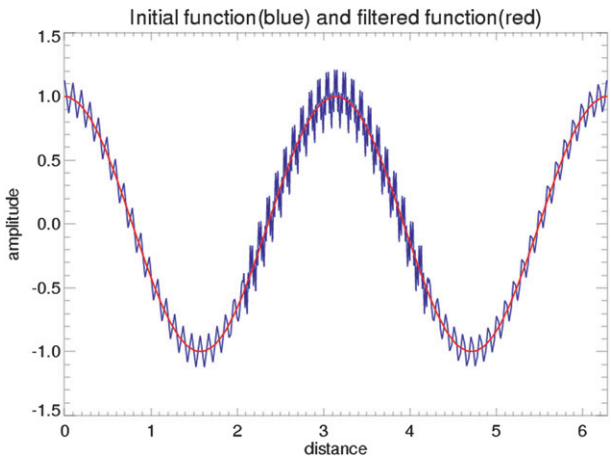

FIG. 13. The initial test function (blue) on the SG1 grid and the filtered field (red). The noise on the entire grid has wavenumber $k_{n_1} = 2\pi/4\Delta x_{\max}$, and the noise on the stretching region and high-resolution area has wavenumber $k_{n_2} = 2\pi/4\Delta x_{\min}$. The convolution filter used a weighting function w_5 with parameters $a = 2\pi/8\Delta x_{\max}$ and $b = 1.5a$, and a truncation distance of $8\Delta x_{\max}$.

function w_5 with parameters ($a = 2\pi/8\Delta x_{\max}$; $b = 1.5a$) and a truncation distance of $8\Delta x_{\max}$. Using appropriate weighting function and truncation distance, the filter is able to eliminate both noises, as we see in Fig. 13.

The ability of the convolution filter to remove noises everywhere on a stretched grid emphasizes the definition of the weighting function independently of the computational mesh. To highlight this property, we use the same test function as in Fig. 13 but with $A_{n_h} = 0$ and $k_{n_1} = 2\pi/2\Delta x_{\max}$. To remove this noise, the convolution filter uses a weighting function w_6 with parameters ($a = 2\pi/8\Delta x_{\max}$; $b = 2.5a$) and a truncation distance of $6\Delta x_{\max}$. Figure 14a shows the initial and the filtered functions; it can be seen that the noise is completely removed everywhere, including in the low-resolution, high-resolution, and stretched zones of the domain. Next, we apply the Shapiro filter to the same test function; as can be seen in Fig. 14b, the noise is completely removed only in the low-resolution zone, and it is only attenuated in the high-resolution and stretched zones. The amount by which the noise is attenuated or removed corresponds to $R(L) = 1 - \sin^2(\pi\Delta x/L)$ where $L = 2\Delta x_{\max} \cong 8\Delta x_{\min}$; because the response depends on the computational gridpoint distance, we conclude that the Shapiro operator is not really appropriate for a variable mesh.

For all tests performed on 1D stretched grids, the convolution filter worked appropriately. With suitable parameter choices, the noise is removed in regions chosen by the user (such as in the stretching zones and/or over the entire domain), the total mass is relatively well conserved, and there is little attenuation of the initial signal. In practice, the choice of the weighting function and truncation distance must be made as a compromise between the cost of the application and the precision of the filter.

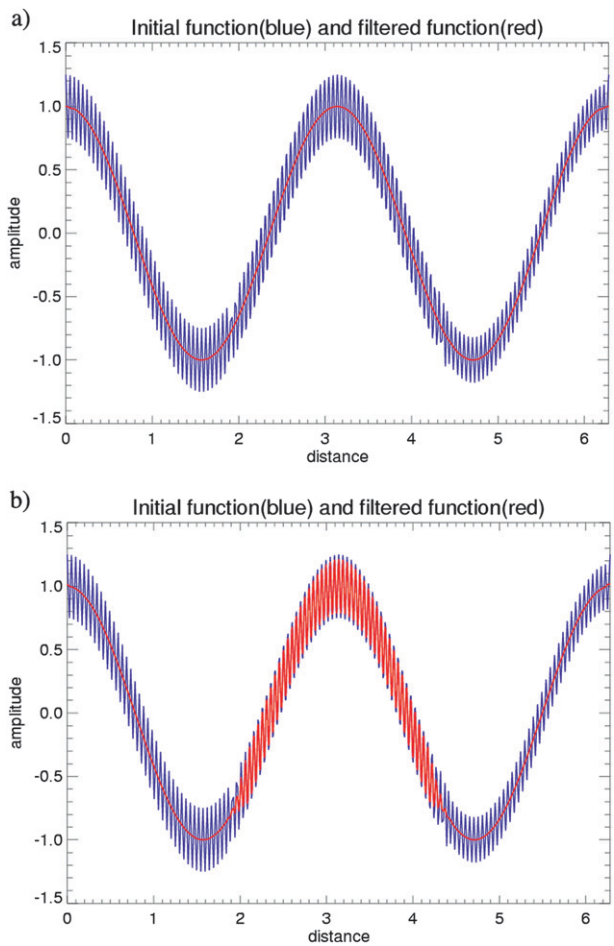

FIG. 14. The initial test function (blue) on the SG1 contains a noise represented on the entire grid with wavenumber $k_{n_1} = 2\pi/2\Delta x_{\max}$. (a) The filtered field (red) is obtained using a convolution filter with a weighting function w_6 with parameters $a = 2\pi/8\Delta x_{\max}$ and $b = 2.5a$, and a truncation distance of $6\Delta x_{\max}$. (b) The filtered field (red) is obtained using the Shapiro filter.

c. *Application of the convolution filter into a 2D Cartesian stretched grid*

The formal approach developed in 1D is generalized for two-dimensional domains. The two-dimensional convolution uses a weighting function that is the product of two one-dimensional functions, similar to those used in the one-dimensional case. The approximation of a 2D convolution using a sequence of 1D convolutions requires reduced computations while producing equally valid analyses when compared with those of the 2D filter scheme as shown by Thatcher and McGregor (2009), who used this approach in the context of a scale-selective filter for dynamical downscaling.

Considering a signal $\psi(x, y)$, the filtered value $\overline{\psi}(x, y)$ is

$$\begin{aligned}\overline{\psi}(x, y) &= (\psi * w)(x, y)\\ &= \int_{-\infty}^{\infty}\int_{-\infty}^{\infty} \psi(s,t)w(x-s, y-t)\,ds\,dt\\ &= \int_{-\infty}^{\infty}\left[\int_{-\infty}^{\infty} \psi(s,t)w_{1\mathrm{D}}(x-s)\,ds\right]w_{1\mathrm{D}}(y-t)\,dt\\ &= \int_{-\infty}^{\infty}(\psi * w_{1\mathrm{D}})(x, t)w_{1\mathrm{D}}(y-t)\,dt\\ &= [(\psi * w_{1\mathrm{D}}) * w_{1\mathrm{D}}](x, y), \end{aligned} \tag{12}$$

where $w(x, y) = w_{1\mathrm{D}}(x)w_{1\mathrm{D}}(y)$, with $w_{1\mathrm{D}}$ representing the same 1D function as in (6). In practice, the 2D filtered function will be obtained conveniently by successive applications of 1D filter in each direction. The weighting function is symmetrical with respect to x and y directions, and also with respect to any line that passes through an application point.

The convolution is expressed as a quadrature for a grid point in the stretched domain as follows:

$$\overline{\psi}(x_i, y_j) = \frac{\sum\limits_{\substack{k\\ d_{i,k}\le d_{\max}}}\ \sum\limits_{\substack{l\\ d_{j,l}\le d_{\max}}} \psi(x_k, y_l)w(d_{j,l})w(d_{i,k})\sigma(x_k)\sigma(y_l)}{\sum\limits_{\substack{k\\ d_{i,k}\le d_{\max}}}\ \sum\limits_{\substack{l\\ d_{j,l}\le d_{\max}}} w(d_{j,l})w(d_{i,k})\sigma(x_k)\sigma(y_l)}, \tag{13}$$

where $d_{i,k}$, $d_{j,l}$, $\sigma(x_k)$, and $\sigma(y_l)$ have the same meaning as in (7). It is important to reiterate that in our proposed convolution filter approach, the weights are calculated using physical distances rather than gridpoint indices. In practice, the width of the weighting function stencil is truncated to a finite distance from the application point when the distance in x or y direction exceeds the maximum prescribed distance $d_{\max}$; this results in an approximately isotropic 2D weighting function.

A 2D stretched grid was built following a similar approach as for the 1D grid. In the center of the mesh is the uniform high-resolution area and, outside of this zone, the grid spacing increases in both directions as a geometric progression with a constant stretching factor of 7.2% until a maximum grid spacing is attained. We chose a total stretching factor $S \approx 4$ in x and y directions, similar to the SG1 previously used in the one-dimension tests.

The purpose of our simplified 2D tests with the convolution filter will be to remove the small scales outside the uniform high-resolution core region of the domain, thus correcting for the anisotropy of a test-function field in the arms-of-the-cross and stretching areas where the resolution varies with direction or the resolution is not uniform.

Similarly to our tests in 1D, we define a test function using 2D sinusoidal waveforms. One will represent a large-scale signal $\psi_l(x, y)$ that will be represented on the entire grid and that we wish to retain with the filter. The second waveform will be a small-scale component $\psi_n(x, y)$ that will be present in the uniform high-resolution region, where it will represent a finescale signal we wish to be retained with the application of the filter; the small-scale component will also be progressively added in the stretching regions, where it will be considered as noise that the filter should remove. The test function will be represented as

$$\psi(x, y) = \psi_l(x, y) + \psi_n(x, y),$$

or for gridpoint representation

$$\psi(x_i, y_j) = A_l \cos(k_l x_i)\cos(l_l y_j) + A_n \cos(k_n x_i)\cos(l_n y_j),$$

where A_l and A_n are arbitrarily set amplitudes, and (k_l, l_l) and (k_n, l_n) are the large-scale and small-scale wavenumbers in x and y directions, respectively. The tests were performed on a grid with a total stretching factor $S \approx 4$ in x and y directions, similar to SG1 previously used in one dimension. The initial field is presented in the upper panel of Fig. 15.

The middle row presents the results using a filter with the weighting function w_1 with parameters ($a = 2\pi/2\Delta x_{\max}$; $b = 1.5a$) and a truncation distance of $d_{\max} = 10\Delta x_{\min}$ (left panel) and $d_{\max} = 21\Delta x_{\min}$ (right panel). We note that the filter successfully removes completely the "noise" when using a large enough truncation distance, and there are no visible deformations of the signal at the borders of the uniform high-resolution area.

The lower row presents the results using a less scale-selective filter with a weighting function w_3 with parameters ($a = 2\pi/2\Delta x_{\max}$; $b = 3a$) with a truncation distance of $d_{\max} = 10\Delta x_{\min}$. The left panel shows the result after one application of the filter, and the right panel after six applications of the filter. The broad spectral response of this filter allows the use of a narrower stencil for the weighting function, but the filter only damps the noise

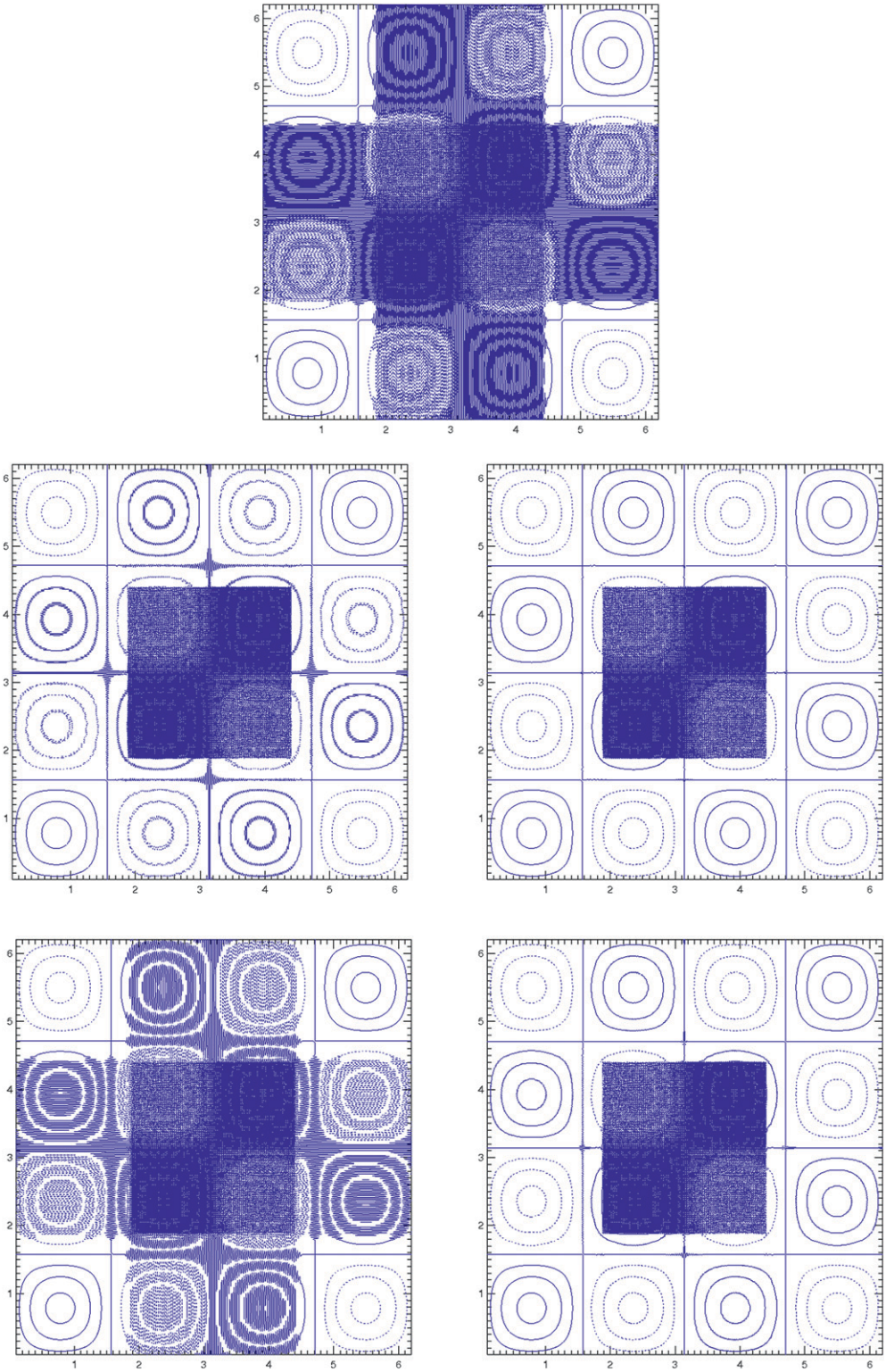

FIG. 15. (top) The initial test field on the 2D stretched grid with $S \cong 4$. (middle) The filtered fields after application of a convolution filter with 1D weighting function w_1 and a truncation distance of (middle left) $10\Delta x_{\min}$ and (middle right) $21\Delta x_{\min}$. (bottom) The filtered fields after application of a convolution filter with 1D weighting function w_4 and a truncation distance $10\Delta x_{\min}$; the result after (bottom left) one and (bottom right) six applications of the filter.

without suppressing it entirely; however, repeated applications of the filter can effectively remove the noise.

4. Conclusions

We described a filtering approach based on the convolution operator that can be applied effectively on stretched grids. The filter can be effective to remove unwanted small scales outside the uniform high-resolution area of the global variable-resolution domain. This approach can be used to render quasi-isotropic fields on variable-resolution grids. The weighting function in the convolution can simply be calculated as the inverse Fourier transform of the spectral response desired for the filter. A key element of the approach is that the weights are based on the physical distance between grid points rather than gridpoint indices; it is this feature that makes this approach attractive for use on variable-resolution grids. The method has here been tested in 1D periodic domain and 2D Cartesian mesh, and on uniform as well as variable-resolution stretched grids.

In the first part of the paper, we presented the mathematical formulation for the convolution filter and an analysis of the weighting function for a uniform periodic one-dimensional domain. We noted that the design of a convolution filter with a sharp cutoff spectral response requires a large number of grid points in the weighting function in order to reproduce the desired response, but such a filter incurs a high computational cost. Truncating the weighting function after some distance can save on computational cost, but the resulting filter only reproduces approximately the desired spectral response, and in general only results in an attenuation of the small scales one wishes to filter. Multiple applications of such an approximate filter can be a pragmatic compromise. We showed that in the simplified context of—a periodic domain, sinusoidal fields, large truncation distance for the weighting function—the convolution filter conserves perfectly the mass, the noise is removed and the large-scale signal is completely preserved.

The second part of the paper was dedicated to the adaptation of the convolution filter for 1D variable-resolution grids. Because the weighting function in the proposed convolution filter depends on the physical distance rather than gridpoint indices, we showed that the response of the filter is almost independent of the stretching of the underlying computational mesh. The only repercussion of the changing resolution is computational—if the application point is located in a high-resolution area, the number of grid points participating in the quadrature is large.

The experiments performed on test functions represented by single harmonics on the one- and two-dimensional periodic stretched grid have shown that the proposed convolution filter can effectively remove completely the small-scale noise while conserving the large-scale signal.

In summary, the proposed approach appears to be a valuable alternative to a conventional gridpoint-based smoothing operator for stretched-grid models. In forthcoming papers, we will expand the present Cartesian-geometry scalar formulation to polar geometry and vectors. The convolution filter approach developed for 1D variable grids and generalized to two-dimensional Cartesian geometry will be adapted for polar geometry as an intermediate step toward a spherical latitude–longitude grid. On the polar grid, the convolution filter will be used not only in the stretching area but also near the poles. As in the present study, we chose for simplicity and efficiency a filter formulation obtained by the separate application of the convolution in radial and azimuthal directions, but preserving the paramount concept of physical distance. Because the number of grid points for a given physical distance in the azimuthal direction varies with radial distances, it will be important to apply first the convolution in azimuthal direction, followed by the application of the convolution in radial direction.

Acknowledgments. This research was done as part of the Doctoral project of the first author and as a project within the Canadian Regional Climate Modelling and Diagnostics (CRCMD) Network, funded by the Canadian Foundation for Climate and Atmospheric Sciences (CFCAS), the Ouranos Consortium for Regional Climatology and Adaptation to Climate Change, and National Centre of Excellence (NCE) Mathematics of Information Technology and Complex Systems (MITACS). Ouranos also provided office space during a large part of this work.

REFERENCES

Bender, C. M., and S. A. Orszag, 1978: *Advanced Mathematical Methods for Scientists and Engineers*. McGraw-Hill, 593 pp.

Bracewell, R. N., 2000: *The Fourier Transform and Its Applications*. 3rd ed. McGraw-Hill, 640 pp.

Caian, M., and J.-F. Geleyn, 1997: Some limits to the variable-mesh solution and comparison with the nested-LAM solution. *Quart. J. Roy. Meteor. Soc.,* **123,** 743–766.

Côté, J., S. Gravel, A. Méthot, A. Patoine, M. Roch, and A. Staniforth, 1997: Preliminary results from a dry global variable-resolution primitive equations model. *Numerical Methods in Atmospheric and Oceanic Modelling: The André J. Robert Memorial Volume,* C. A. Lin, R. Laprise, and H. Ritchie, Eds., Canadian Meteorological and Oceanographic Society, 245–259.

——, ——, ——, ——, ——, and ——, 1998: The operational CMC–MRB Global Environmental Multiscale (GEM) model. Part I: Design considerations and formulation. *Mon. Wea. Rev.,* **126,** 1373–1395.

Courtier, P., and J.-F. Geleyn, 1988: A global numerical weather prediction model with variable resolution: Application to the shallow-water equations. *Quart. J. Roy. Meteor. Soc.,* **114,** 1321–1346.

Déqué, M., and J. P. Piedelièvre, 1995: High resolution climate simulation over Europe. *Climate Dyn.,* **11,** 321–339.

Fox-Rabinovitz, M. S., G. L. Stenchikov, M. J. Suarez, and L. L. Takacs, 1997: A finite-difference GCM dynamical core with a variable-resolution stretched grid. *Mon. Wea. Rev.,* **125,** 2943–2968.

——, E. H. Berbery, L. L. Takacs, and R. C. Govindaraju, 2005: A multiyear ensemble simulation of the U.S. climate with a stretched-grid GCM. *Mon. Wea. Rev.,* **133,** 2505–2525.

——, J. Côté, B. Dugas, M. Déqué, and J. L. McGregor, 2006: Variable resolution general circulation models: Stretched-Grid Model Intercomparison Project (SGMIP). *J. Geophys. Res.,* **111,** D16104, doi:10.1029/2005JD006520.

——, ——, ——, ——, ——, and A. Belochitski, 2008: Stretched-grid Model Intercomparison Project: Decadal regional climate simulations with enhanced variable and uniform-resolution GCMs. *Meteor. Atmos. Phys.,* **100,** 159–177.

Gibelin, A. L., and M. Déqué, 2003: Anthropogenic climate change over the Mediterranean region simulated by a global variable resolution model. *Climate Dyn.,* **20,** 327–339.

Laprise, R., 2008: Regional climate modelling. *J. Comput. Phys.,* **227,** 3641–3666.

McGregor, J. L., K. C. Nguyen, and J. J. Katzfey, 2002: Regional climate simulations using a stretched-grid global model. Research Activities in Atmospheric and Oceanic Modelling, WMO Tech. Doc. 1105, Rep. 32, 3.15–3.16.

Schmidt, F., 1977: Variable fine mesh in the spectral global models. *Beitr. Phys. Atmos.,* **50,** 211–217.

Shapiro, R., 1970: Smoothing, filtering, and boundary effects. *Rev. Geophys. Space Phys.,* **8,** 359–387.

Surcel, D., 2005: Filtres universels pour les modèles numériques à résolution variable. M.S. thesis, Dept. of Earth and Atmospheric Sciences, Université du Québec à Montréal, 104 pp.

Takacs, L., W. Sawyer, M. J. Suarez, and M. S. Fox-Rabinovitz, 1999: Filtering techniques on a stretched grid general circulation model. NASA Tech. Memo. 104606, Vol. 16, 45 pp. [Available from Data Assimilation Office, NASA GSFC, Greenbelt, MD 20771.]

Thatcher, M., and J. L. McGregor, 2009: Using a scale-selective filter for dynamical downscaling with the Conformal Cubic Atmospheric Model. *Mon. Wea. Rev.,* **137,** 1742–1752.

Yessad, K., and P. Bénard, 1996: Introduction of a local mapping factor in the spectral part of the Météo-France global variable mesh numerical weather forecast model. *Quart. J. Roy. Meteor. Soc.,* **122,** 1701–1719.

Zadra, A., D. Caya, J. Cote, B. Dugas, C. Jones, R. Laprise, K. Winger, and L.-P. Caron, 2008: The next Canadian Regional Climate Model. *Phys. Canada,* **64,** 75–83.